ACS Energy LETTERS

http://pubs.acs.org/journal/aelccp

Interfacial Engineering with a Hole-Selective Self-Assembled Monolayer for Tin Perovskite Solar Cells via a Two-Step Fabrication

Donghoon Song, Sudhakar Narra, Meng-Yu Li, Jian-Sing Lin, and Eric Wei-Guang Diau*

Cite This: *ACS Energy Lett.* 2021, 6, 4179–4186

Read Online

ACCESS | Metrics & More | Article Recommendations | Supporting Information

ABSTRACT: This work is the first report on a hole-selective tin-based perovskite solar cell (PSC) using the concept of a self-assembled monolayer (SAM) to modify the ITO surface to fabricate a uniform tin perovskite layer via a two-step sequential deposition method. Herein, we developed a preheating procedure to diminish effectively the amounts of hydroxyl groups and oxygen vacancies on the ITO surface to produce a uniform SAM. The ITO substrate preheated at 400 °C gave the best device performance for an efficiency of power conversion (PCE) reaching 6.5%, and 80% of the initial PCE was maintained in a glovebox for ∼1900 h. Electrochemical impedance spectra and time-resolved spectra were used to understand the interfacial charge recombination and hole-extraction kinetics in relation to the observed device performance. The present work thus provides a new direction for the development of SAM-based lead-free perovskite solar cells for their future scaled-up production.

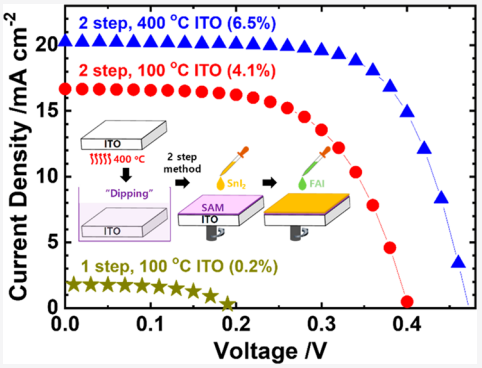

By virtue of its low toxicity as well as a broad range of light absorption, a large charge-carrier mobility, and hence high theoretical efficiency, lead-free tin perovskite solar cells (PSCs) are deemed a sustainable, promising, and renewable technology.[1−3] In tin PSCs, two challenges lie ahead: improving device performance and stability to demonstrate their large-area scalability. Although the certified efficiency of power conversion (PCE) of lead PSCs has reached beyond ∼25%,[4] recent efforts have made tin PSCs exceeding 14%.[5,6] Unlike lead PSCs, inverted planar *p*-type architectures for tin PSCs are mostly chosen. For example, a typical tin PSC has the device structure ITO/PEDOT:PSS/$FASnI_3$/C60/BCP/Ag.[7] For most tests, tin perovskites such as $FASnI_3$ were deposited with a one-step method that entails sophisticated injection of antisolvents in a narrow processing window (presumably less than ±1 s).[1−3] This narrow injection window thus becomes a critical issue for tin perovskites that suffer from a small energy of defect formation, rapid crystallization, and reaction between tin halide and organic ammonium salts.[8] We developed a two-step method[9] to fabricate tin perovskites over a wide processing window (typically greater than ±5 s).[9] We believe that this two-step method is well-suited to scale up tin PSCs for its great feature of varying the device configuration to attain the best device performance for future commercialization.

Tin perovskites possess abundant defect states and shallow energy levels (e.g., by 0.2−0.6 eV for VBM and 0.5−0.7 eV for CBM).[2] Central to precedented research is protecting perovskites against Sn^{2+} oxidation to defective Sn^{4+} through exploring various additives,[10−13] cations,[14−19] alloying,[20] or (pseudo)halides[21,22] and through retarding their rapid crystallization with additives[23] or through a solvent-mediated intermediate (e.g., a tin iodide (SnI_2)−dimethyl sulfoxide (DMSO) complex).[24,25] In contrast, little research has been reported on replacing of hole- or electron-transport material (represented by HTM or ETM, respectively) with novel materials to enhance further the rate of charge transport to improve the PCE. It is worth noting that upon applying an indene-C_{60} bisadduct (ICBA) to replace conventional C_{60} serving as ETM, the photovoltage of the device was significantly enhanced by as much as 0.3 V for a tin PSC.[26] High-performance HTMs such as spiro-OMeTAD and PTAA that are intensively utilized in lead-based PSC have not been reported for tin-based PSCs; only PEDOT:PSS and NiO_x were reported because of the interfacial problem between the HTM and tin perovskite that hinders the formation of a uniform perovskite layer.[27] Inherent properties including parasitic light

Received: September 29, 2021
Accepted: October 27, 2021
Published: November 3, 2021

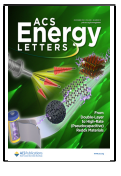

https://doi.org/10.1021/acsenergylett.1c02124
ACS Energy Lett. 2021, 6, 4179−4186

absorption, ohmic drop loss, rigidity in energy levels and mechanical properties, nonconformal contact, and limited scalability challenge these two HTMs.[28,29] Furthermore, thermal and optoelectrochemical vulnerability of PEDOT:PSS and oxidative NiO_x limit the further development of tin-based PSCs;[30] searching for new replacements is another alternative.

A self-assembled monolayer (SAM) has been extensively studied because of its simple processing using spin-coating or dipping or vapor deposition, for not only optoelectronic applications, including solar cells, light-emitting diodes, transistors, and sensors, but also fundamental studies of electrochemistry, biology, and electronics and synthesis of nano- or microparticles.[31,32] Energy levels tunable over a wide range could allow SAMs to serve as an interlayer for hole or electron selection in PSCs. In addition, SAMs are promising photovoltaic materials because of their molecular designability, excellent mechanical flexibility, no need of dopants, negligible loss of light transmittance, large-area scalability, and almost conformal and loss-less electrical contacts.[33] To date, several SAMs have been explored for lead-based PSCs;[33] they were mostly used in settling onto metal oxides such as TiO_2, SnO_2, or ZnO for the purposes of passivating the surfaces, enlarging perovskite crystals, prolonging operational stability, or catalyzing charge selectivity. A SAM served as a hole-selected interlayer for lead PSCs to attain a PCE as great as 20%.[33] Surface states on indium tin oxide (ITO) glasses play a crucial role to anchor the SAM, as well as to modulate charge transfer and recombination and to utilize efficiently visible and near-infrared photons.[34,35] Tailoring ITO surface states with a suitable SAM has, however, gained little attention.

A SAM is categorized as a 2D material. Self-assembly is thermodynamically favorable and is assumed to occur on an ITO surface with appropriately selected molecules.[31−33] SAM can alter the property of an ITO surface from heterogeneous to homogeneous,[32] offering even hole selectivity. In the present work, we selected three SAM molecules, [2-(9*H*-carbazol-9-yl)ethyl]phosphonic acid (2PACz), [2-(3,6-dimethoxy-9*H*-carbazol-9-yl)ethyl]phosphonic acid (MeO-2PACz), and 3,6-dimethyl-9H-carbazol-9-yl)butyl]phosphonic acid (Me-4PACz),[36,37] to modify the surface of ITO for the fabrication of a uniform tin perovskite layer through a two-step approach.[9] We found that the traditional one-step method[11,17,19] failed to fabricate a uniform perovskite layer on the SAM surface and gave a poor device performance. In contrast, tin perovskite films of satisfactory quality were produced on the SAM/ITO substrate using the two-step method. The device made of dip-coating MeO-2PACz SAM free of HTM exhibited the best performance. We found also that the annealing temperature of the ITO substrate plays a crucial role in the formation of a SAM, charge transport, and charge recombination in the tin PSC characterized by electrochemical impedance spectroscopy (EIS) and time-resolved spectral investigations using time-correlated single-photon-counting (TCSPC) and femtosecond transient absorption spectral (TAS) techniques. The MeO-2PACz device with ITO annealing temperature of 400 °C exhibited an impressive PCE of 6.5% with excellent long-term stability (~80% retention of initial performance after ~1900 h) without encapsulation.

As Figure 1 shows, 2PACz, MeO-2PACz, and Me-4PACz all have phosphonic acid as an anchoring group, a hydrocarbon chain as a spacer group, a carbazole moiety as a hole-selective group, and a methoxy or methyl side chain as a terminal group. In particular, the specific interaction between Sn^{2+} and the

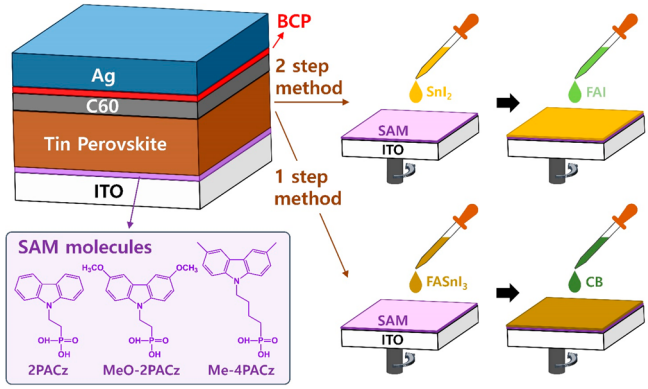

Figure 1. Schematic demonstration of a device configuration of a tin-based PSC showing two perovskite deposition methods and three SAM molecules—2PACz, MeO-2PACz, and Me-4PACz—as the corresponding chemical structures indicate. In the one-step deposition, the $FASnI_3$ was directly spin-coated, during which an antisolvent chlorobenzene (CB) was injected. In the two-step deposition, the SnI_2 in DMSO and FAI in a cosolvent system were sequentially deposited using spin-coating to form $FASnI_3$.

methoxy group in MeO-2PACz would be capable of suppressing Sn^{2+} oxidation and serving as a template for growth of the perovskite crystal.[33] While phosphonic acid contributes to tight anchoring of SAM molecules onto an ITO surface by ester linking or hydrogen bonding, a spacer group helps their dense packing by lateral interaction, and a terminal group is responsible for surface properties and interaction with perovskites.[31−33] The dipolar moment of a SAM would determine the energy levels of CBM and VBM with respect to vacuum. The VBM values for a SAM formed from 2PACz, MeO-2PACz, and Me-4PACz have been reported to be −5.6, −5.1, and −5.8 eV, respectively.[36,37] Given that tin perovskite $FASnI_3$ has a VBM as shallow as −4.9 eV stemming from the electrons at Sn 5s weakly bound by the nuclear charge,[2] the VBM of PEDOT:PSS remains −5.0 eV, which is near that of MeO-2PACz, likely boding well for excellent charge transfer.

Figure 1 illustrates an architecture of SAM-based PSC (ITO/SAM/$FASnI_3$/C60/BCP/Ag) in which the chemical structures of the SAM, and the one- and two-step deposition methods are shown. Excellent film formation was reported for lead perovskites on these SAMs.[36,37] For tin perovskites, however, DMSO instead of DMF was used as a precursor solvent for one-step deposition, which differs from lead perovskites because DMSO has a higher boiling point and superior coordination affinity with SnI_2 to retard crystallization and hence produce an effective film morphology.[24] In addition, DMSO possesses a great solubility for an essential additive, tin fluoride (SnF_2), to fabricate high-performance tin-based PSCs.[24,25]

In our SAM approach, we attached SAMs onto ITO substrates upon dipping the substrates in a MeO-2PACz ethanolic solution (0.2 M) for 12 h. We then measured water-contact angles of SAM on ITO substrates and that of PEDOT:PSS for comparison. The results (Figure S1) indicate that PEDOT:PSS is strongly hydrophilic because of the hydrophilic PSS enriched on the surface.[38,39] MeO-2PACz is the most hydrophilic among all three SAMs: the hydrophilicity follows the order PEDOT:PSS (<10°) ≫ MeO-2PACz (55°) > 2PACz (72°) > Me-4PACz (83°), being prominently affected by the end-group property. PEDOT:PSS has hence served as a suitable HTM for tin-based PSCs, almost

https://doi.org/10.1021/acsenergylett.1c02124
ACS Energy Lett. 2021, 6, 4179−4186

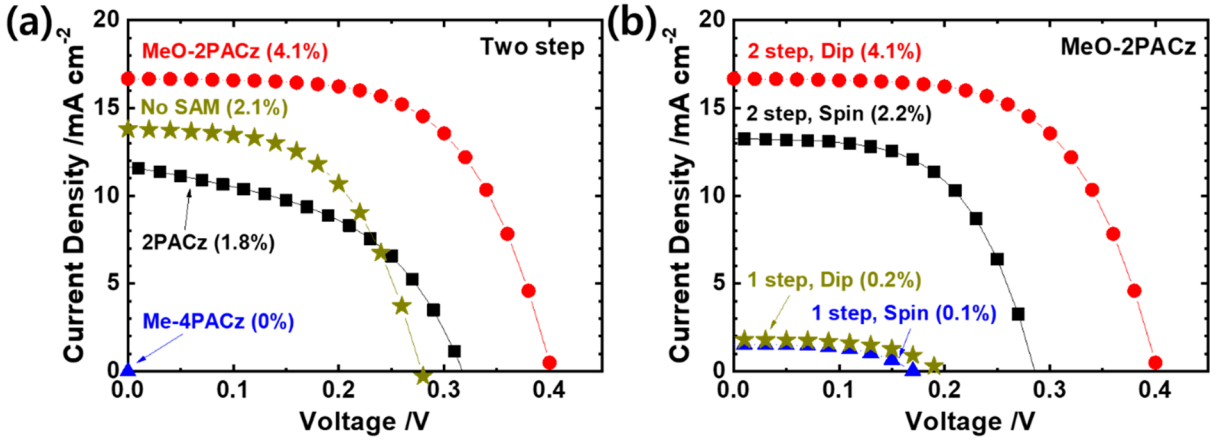

Figure 2. Representative $J-V$ characteristic curves of tin perovskite solar cells fabricated via (a) SAM of varied types on ITO with the dipping method according to a two-step approach and (b) varied SAM deposition methods (dipping vs spin-coating) according to perovskite preparations (two-step vs one-step) using MeO-2PACz as SAM. The preheating temperature of the ITO substrate is 100 °C.

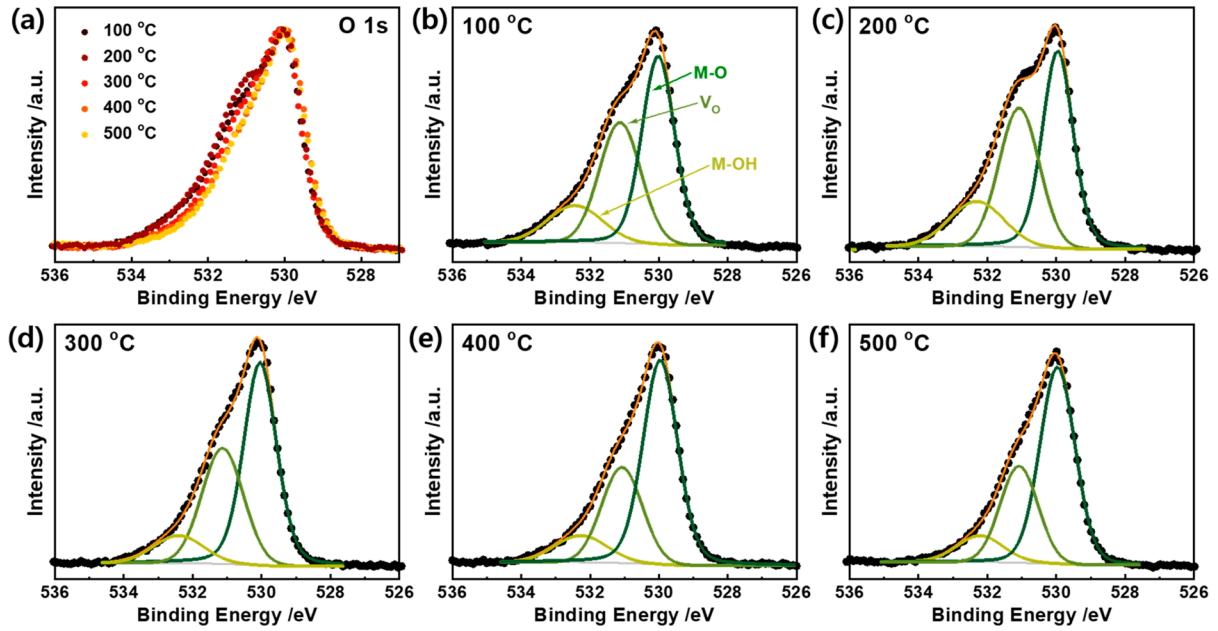

Figure 3. XPS of O 1s obtained from ITO substrates preheated at (a) 100−500 °C with the individual spectra showing the deconvoluted components for (b) 100 °C, (c) 200 °C, (d) 300 °C, (e) 400 °C, and (f) 500 °C preheated ITO substrates, showing relative signals for M-O (oxides, ∼530.0 eV), V_O (oxygen vacancy, ∼531.1 eV), and M−OH (hydroxyl, ∼532.3 eV). The area ratios of V_O over M−OH were calculated to be 0.745/0.299, 0.829/0.361, 0.647/0.184, 0.495/0.179, and 0.494/0.177 from 100 to 500 °C, respectively.

exclusively reported in the literature.[1−3] Hole transport loss is negligible in a SAM because it forms only a single molecular layer on the ITO surface,[31−33] whereas the thicker film (∼50 nm) of PEDOT:PSS could retard hole transport, giving rise to charge accumulation at the interface for possible charge recombination.[40] For the characteristic plots of current density versus voltage shown in Figure S2a, PEDOT:PSS suffers from loss in charge transport to an appreciable extent in comparison with the SAM. Furthermore, light harvesting in a long wavelength region (650−900 nm) can be significantly depressed in tin PSCs;[41] light absorption loss by the HTM hence requires improvement. According to the transmittance spectra shown in Figure S2b, the SAMs dissipate only slightly the near-infrared light transmittance, whereas PEDOT:PSS decreases transmittance by 1−6% over the wavelength region 700−1200 nm.

To investigate which SAM fits best for tin PSCs, we deposited $FASnI_3$ perovskites over the SAM on applying a two-step method reported elsewhere.[9] In the first step, SnI_2 (0.8 M), SnF_2 (0.16 M), and $EDAI_2$ (0.008 M) were dissolved in DMSO; in the second step, FAI (20 mg) was dissolved in IPA/hexafluoro-2-propanol (HFP)/chlorobenzene (CB) (volume ratio: 5:5:2) (1.2 mL); the FAI loading time was 40 s. We found that the more hydrophilic the SAM, the better the perovskite film formed. Accordingly, the devices made of the Me-4PACz SAM exhibited almost zero performance (see the result in Figure 2a). The 2PACz device attained PCE 1.8%, which is poorer than the device made with no SAM (PCE = 2.1%). In contrast, MeO-2PACz permitted the best formation of a perovskite film among the SAMs through the satisfactory hydrophilicity and, likely, the interaction between SnI_2 and the methoxy group. Accordingly, the MeO-2PACz device attained PCE 4.1%, providing a successful demonstration of the hole-

https://doi.org/10.1021/acsenergylett.1c02124
ACS Energy Lett. 2021, 6, 4179−4186

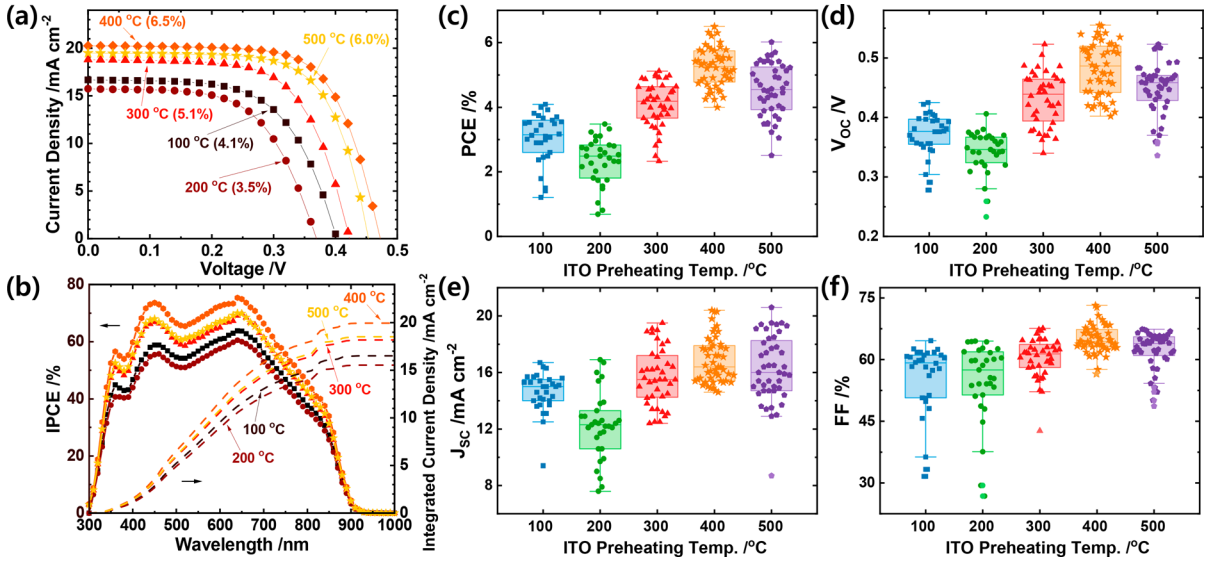

Figure 4. (a) Representative $J-V$ curves and (b) corresponding IPCE spectra of a MeO-2PACz device with varied ITO preheating temperatures, 100−500 °C. Statistical distributions of (c) PCE, (d) V_{OC}, (e) J_{SC}, and (f) FF were obtained from more than 30 devices for each temperature condition.

extraction ability of a SAM because of the satisfactory quality of the perovskite film together with the energy levels well-matched to $FASnI_3$.

This SAM approach fails for a tin-based PSC fabricated according to a conventional one-step method. As shown in Figure 2b and Table S2, the one-step MeO-2PACz devices attained PCE of merely 0.1% and 0.2% using the spin-coating and dipping methods to prepare the SAM sample, respectively. Our results indicate that uniform tin perovskite films cannot be produced on top of a SAM with the one-step method because of the highly hydrophobic nature of the surface of the SAM. In contrast, our two-step approach has the flexibility to spread SnI_2 evenly on top of the SAM and then to react with FAI forming a uniform perovskite layer for the device to work. As a result, using a spin-coating method with MeO-2PACz solution[36,37] (1.0 M) to prepare the SAM sample followed by a two-step deposition method resulted in PCE 2.2%, which is significantly less than that prepared with the dipping method; the performance of the former device is similar to that for the device without the SAM. The MeO-2PACz device prepared via the dipping and two-step methods attained the best performance (PCE = 4.1%), outperforming the devices prepared with other methods.

We then closely inspected the surface of ITO and its interaction with the SAM molecules. According to the literature,[34] hydroxyl groups such as in $In(OH)_3$ are abundant on an ITO surface, which promote haphazard anchoring of SAM molecules, presumably to form clusters or to suppress reorientation;[42,43] furthermore, $In(OH)_3$ might be randomly oriented and loosely bound to the ITO lattice. The latter might weaken charge transfer, and the former hinder normal orientation of SAMs and hence alter the surface properties. As a result, removing undesirable hydroxyls is crucial for the formation of a uniform and cluster-free SAM film and ultimately to promote the device performance. We therefore sought the best surface of the ITO through tailoring the amounts of hydroxyls with thermal pretreatment that can trigger dehydration of $In(OH)_3$ by increasing the temperature toward that at which a transformation to oxide such as In_2O_3 might occur.[44]

For a systematic study, we selected five temperatures between 100 and 500 °C with increment 100 °C to anneal the ITO substrate for 30 min under ambient air before SAM anchoring. ITO was heated at 100 °C as a standard for the results shown in Figure 2; a temperature above 600 °C caused structural deformation and bending of the ITO substrates. Figure S3 shows SEM images for the morphologies of the ITO substrates preheated under these five temperatures; no distinguishable morphological feature was observed for these pretreatments. Figures 3 and S4 show the high-resolution X-ray photoelectron spectroscopy (XPS) spectra of the O 1s species on the surface (no etching) and bulk states (measured after ∼30 s of Ar etching), respectively. No change for the components on the O 1s species was observed in the bulk states. In contrast, the peak intensity of hydroxyls at binding energy of ∼532.3 eV on the surface was increased upon increasing the temperature from 100 to 200 °C, gradually decreased to 400 °C, and maintained the same level at 500 °C. The variation of the component corresponding to the oxygen vacancy at binding energy ∼531.1 eV was similar to that of hydroxyls, as shown in Figure 3. The decrease of oxygen vacancies upon annealing was observed because annealing in ambient air conditions can repair oxygen vacancies as reported elsewhere.[35] In particular, the repaired oxygen vacancy concomitantly modified the principal optoelectrical properties on weakening the Burstein−Moss effect, as evident from a systematically narrowing band gap (Figure S5) and altering sheet resistance (Table S3). More importantly, a great broadening in the transmittance spectra in the 800−1500 nm region (Figure S5) was triggered from preheating ≥400 °C, desirable for a small band gap device like tin PSC to enhance its light-harvesting ability.

Using the ITO preheated at 100−500 °C, the corresponding $J-V$ characteristic curves of the MeO-2PACz devices are shown in Figure 4a. A pronounced effect of the ITO preheating on photovoltaic performance is discernible; the device performance corresponds to the preheating temperature

https://doi.org/10.1021/acsenergylett.1c02124
ACS Energy Lett. 2021, 6, 4179−4186

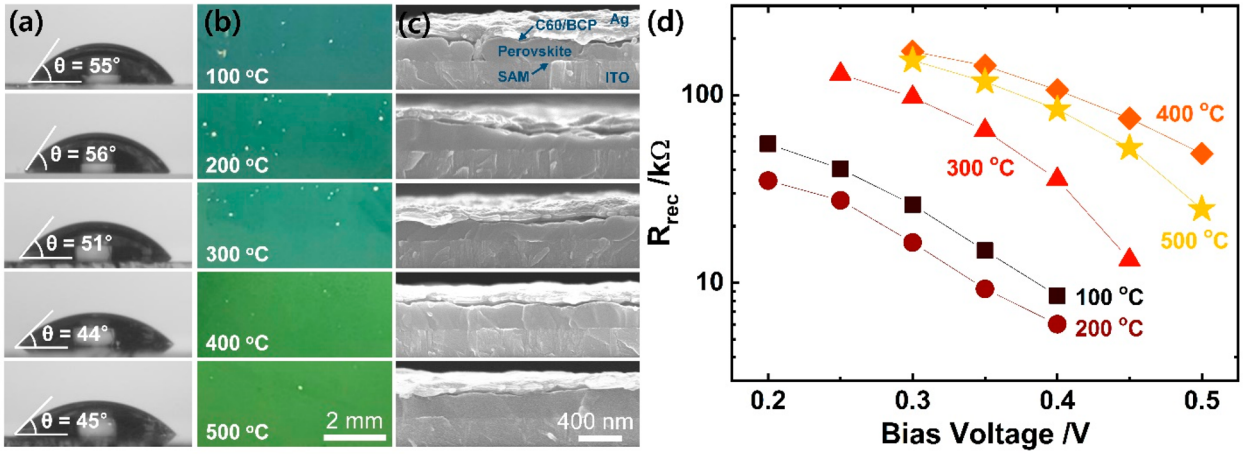

Figure 5. Investigation of ITO preheating effects on (a) water contact angles of ITO/MeO-2PACz substrates, (b) optical images taken at the ITO glass side of tin PSC, and (c) cross-sectional SEM images of devices for T = 100 to 500 °C as indicated. (d) Charge recombination resistance as a function of bias voltage obtained from the EIS measurements for the devices made with ITO preheating temperatures 100−500 °C.

with order 400 > 500 > 300 > 100 > 200 °C; the 400 °C device attained PCE 6.5%; the 500 °C device also exhibits a PCE reaching 6.0%. The 200 °C device suffered from the greatest extent of oxygen vacancies and OH functional groups to yield the poorest device performance (PCE = 3.5%). The efficiency spectra of incident photon-to-current conversion (IPCE) shown in Figure 4b reveal excellent agreement between J_{SC} in Figure 4a and integrated J_{SC} over the measured wavelengths in all cases. The effects of hysteresis of the MeO-2PACz devices at 100 and 400 °C were negligible according to the $J-V$ curves shown in panels a and b of Figure S6, respectively. The current densities of the PEDOT:PSS and MeO-2PACz devices under one-sun irradiation at the maximum power point were stable for 5000 s, as shown in panels a and b of Figure S7, respectively. We fabricated more than 30 devices for each SAM to compare their performance reproducibility; the statistical distributions of each photovoltaic parameter appear in Figure 4c−f, and their corresponding values are listed in Tables S4−S8. The preheating effect to modify the ITO surface was confirmed for the PEDOT:PSS device fabricated using a one-step method, for which the device performance was promoted from PCE 6.5 to 7.1% when the ITO annealing temperature was increased from 100 to 400 °C (Figure S8).

As this report is the first on SAM-based tin PSCs, the long-term operational stability is a challenging issue. Reported time spans for tin perovskite solar cells are generally less than ∼1000 h despite the varied test conditions.[33] Figure S9 shows the enduring stability of the 400 °C devices without encapsulation stored in a glovebox; ∼80% of initial PCE was retained after shelf storage for ∼1900 h. Taking into account that the minute amount of humid air unavoidable during fabrication even in a glovebox can incrementally impair tin perovskites, this stability result is inspiring.

To scrutinize the effect of the ITO preheating temperature affecting the device performance, we implemented contact-angle and morphological measurements for SAM and perovskite films. As shown in Figure 5a, the contact angle of the SAM film was slightly increased from 100 to 200 °C, then decreased from 200 to 400 °C, and slightly increased again to 500 °C. The preheating thus has an effect to enhance the surface hydrophilicity to attain an optimal condition at 400 °C, presumably as a result of cluster-tolerant film formation or normal orientation. Optical images shown in Figure 5b reveal that small granular-like white spots (i.e., defects) in perovskite films become pronounced for $T \leq 300$ °C, whereas they were greatly depressed for $T \geq 400$ °C. Figure 5c shows cross-sectional SEM images at varied preheating temperatures. The thickness of the perovskite film was clearly not uniform for $T \leq 300$ °C, whereas smooth and thicker perovskite films were produced for $T \geq 400$ °C. Top-view SEM images shown in Figure S10 indicate that preheating results in producing larger crystals for $T \geq 400$ °C. This result is akin to the SAM template effect for the lead-perovskites reported elsewhere.[33] Considering the above results, we imagine that modulating the amount of excessive hydroxyls for $T \approx 400$ °C is fundamental for the formation of defect-tolerant and uniformly thick perovskite films. We emphasize that, despite the decrease of hydroxyls on preheating at $T \geq 400$ °C, the amount of MeO-2PACz anchored on the ITO surface is still enough to serve as a smooth buffer layer for a perovskite layer of high quality to be produced on it.

Electrochemical impedance spectroscopy serves as a nondestructive and powerful tool that is frequently utilized in PSCs to examine the kinetics of charge transport and recombination.[45] We recorded EIS spectra for the MeO-2PACz devices with T = 100−500 °C in darkness upon varying the bias voltage over 0.2−0.5 V with voltage amplitude of 10 mV for frequencies in the in range of 1 MHz−1 Hz. The full sets of Nyquist plots are shown in Figure S11; they were fitted using a suitable equivalent- circuit model. Two semicircles in a Nyquist plot are typically observed from a mesoporous tin PSC; the first and second semicircles are correlated to charge transfer and charge recombination at the perovskite interface, respectively.[21,41] The first semicircle was absent in the SAM-based tin PSC, presumably because of rapid charge transfer;[46] it can be associated with high-performance tin PSCs.[11,41] We therefore correlated the dominant semicircle shown in Figure S11 with charge recombination. After analysis of these Nyquist plots, the charge recombination resistance is shown as a function of bias voltage in Figure 5d. The recombination resistance shows a trend following the order 400 > 500 > 300 > 100 > 200 °C, consistent with the trend on device performance (in particular V_{OC}) (Figure 4a). The device for T = 400 °C

https://doi.org/10.1021/acsenergylett.1c02124
ACS Energy Lett. 2021, 6, 4179−4186

attained the greatest resistance, benefiting from the excellent interfacial property between the SAM and perovskite layers, and decreased surface states for retarded charge recombination.[44] Further charge transport and recombination kinetics were investigated using TCSPC and femtosecond TAS techniques detailed in the following.

ITO is an *n*-type degenerate semiconductor and forms an electron−hole recombination junction with an HTM for charge transfer.[47] The surface states due to oxygen vacancy are likely located near the CBM of ITO and hence affect the charge-transfer characteristics. We thus performed measurements of steady-state photoluminescence (PL) and TCSPC with the ITO/perovskite and ITO/SAM/perovskite samples. Panels a and b of Figure S12 show the PL and TCSPC results for these two samples at varied ITO preheating temperatures, respectively. The PL intensities of the ITO/perovskite samples show a systematically increasing trend upon increasing the preheating temperature (as shown in Figure S13a). This phenomenon is explicable as the increasing of film thickness of perovskite upon increasing ITO preheating temperature. In contrast, the fitted TCSPC time coefficients presented in Table S9 indicate a decreasing trend upon increasing the ITO preheating temperature, which can be rationalized as the produced perovskite films involve defects in the bulk and in the grain surface at higher preheating temperatures (refer to the detailed discussion in the Supporting Information).

On the basis of the TCSPC results of the ITO/perovskite samples, we found that the ITO preheating processing might lead to a poor crystal growth of perovskite. The information on interfacial charge-recombination kinetics, however, was unobtainable because of insufficient time resolution for the TCSPC measurements. For this reason, we carried out femtosecond TAS experiments for the ITO/perovskite samples; a detailed description and discussion of the TAS results (Figure S13 and Table S10) are given in the Supporting Information. In summary, we found that ITO preheating helps to retard the interfacial charge recombination as the optimal condition occurs at T = 400 °C, consistent with the XPS results (Figure 3) showing the decreased OH groups and oxygen vacancies on the ITO surface upon increasing the preheating temperature.

When the SAM was present between ITO and the perovskite layer, the PL of the perovskite was significantly quenched (Figure S12a) because of the efficient effect of charge extraction assisted by the SAM. The TCSPC results shown in Figure S12b and Table S9 indicate that the average PL lifetimes greatly decreased in the presence of a SAM. The preheating also assisted the charge extraction for τ_{avg} = 4.1 ns at T = 100 °C, gradually decreasing to τ_{avg} = 2.6 ns at T = 400 °C; preheating the ITO to 500 °C raised τ_{avg} to 5.0 ns because of the enhanced contribution from the slow component, presumably assigned to the shallow trap-mediated recombination analogous to lead-based perovskites. Hole extraction was, however, significantly enhanced in the presence of the SAM for all samples so that the retardation of the extraction kinetics at T = 500 °C might be rationalized to be due to an enhanced sheet resistance upon increasing the preheating temperature (Table S3). As a result, the sample for T = 400 °C exhibited an excellent hole-extraction ability to attain the best device performance.

In conclusion, we report a new concept to modify the ITO surface using a self-assembled monolayer for fabrication of hole-selective tin perovskite solar cells without HTM PEDOT:PSS or NiO_x. We identified the most promising SAM, MeO-2PACz, dipped on the ITO substrate with a satisfactory hydrophilic property to deposit a perovskite layer according to a two-step sequential procedure. The conventional one-step approach cannot produce a uniform perovskite film because of the uneven nucleation and rapid crystallization of the tin perovskite crystal on the SAM surface, which is less hydrophilic than the PEDOT:PSS surface. In the two-step approach, however, the hydrophilicity on the ITO/SAM surface plays an important role in the interaction of the SAM with SnI_2 for the SnI_2/DMSO precursor evenly spread on the ITO substrate to react with the FAI/cosolvent precursor with a controllable loading time. To decrease the extent of OH groups and oxygen vacancies for feasible attachment of the SAM, the ITO substrates were preheated from 100 to 500 °C; this procedure significantly enhanced the hydrophilicity of the ITO/SAM surface for a uniform tin perovskite film to be produced. With the optimal preheating condition at T = 400 °C, the device performance was promoted to PCE 6.5% with a device enduring stability attaining 80% of initial PCE for ∼1900 h without encapsulation. EIS, TCSPC, and femtosecond TAS techniques were employed to study the interfacial charge transport, charge recombination, and hole-extraction kinetics to promote an understanding of the key parameters controlling the device performance for this new series of tin perovskite solar cells. We believe that this novel technique reported herein will open a new door for future development on HTM-free lead-free perovskite solar cells.

■ ASSOCIATED CONTENT

Supporting Information

The Supporting Information is available free of charge at https://pubs.acs.org/doi/10.1021/acsenergylett.1c02124.

Experiments; current−voltage characteristics; contact angles; XPS, SEM, OM, PL, TCSPC, TAS, and EIS results (PDF)

■ AUTHOR INFORMATION

Corresponding Author

Eric Wei-Guang Diau − *Department of Applied Chemistry and Institute of Molecular Science, National Yang Ming Chiao Tung University, Hsinchu 30010, Taiwan; Center for Emergent Functional Matter Science, National Yang Ming Chiao Tung University, Hsinchu 30010, Taiwan;* orcid.org/0000-0001-6113-5679; Email: diau@nycu.edu.tw

Authors

Donghoon Song − *Department of Applied Chemistry and Institute of Molecular Science, National Yang Ming Chiao Tung University, Hsinchu 30010, Taiwan;* orcid.org/0000-0003-0914-1507

Sudhakar Narra − *Department of Applied Chemistry and Institute of Molecular Science, National Yang Ming Chiao Tung University, Hsinchu 30010, Taiwan; Center for Emergent Functional Matter Science, National Yang Ming Chiao Tung University, Hsinchu 30010, Taiwan;* orcid.org/0000-0003-4893-9204

Meng-Yu Li − *Department of Applied Chemistry and Institute of Molecular Science, National Yang Ming Chiao Tung University, Hsinchu 30010, Taiwan*

https://doi.org/10.1021/acsenergylett.1c02124
ACS Energy Lett. 2021, 6, 4179−4186

Jian-Sing Lin − *Department of Applied Chemistry and Institute of Molecular Science, National Yang Ming Chiao Tung University, Hsinchu 30010, Taiwan*

Complete contact information is available at: https://pubs.acs.org/10.1021/acsenergylett.1c02124

Notes

The authors declare no competing financial interest.

■ ACKNOWLEDGMENTS

Taiwan Ministry of Science and Technology (MOST 110-2123-M-A49-001 and MOST 110-2634-F-009-026) and Center for Emergent Functional Matter Science of National Yang Ming Chiao Tung University (NYCU) from The Featured Areas Research Center Program within the framework of the Higher Education Sprout Project by Taiwan Ministry of Education (MOE) supported this research.

■ REFERENCES

(1) Diau, E. W.-G.; Jokar, E.; Rameez, M. Strategies to improve performance and stability for tin-based perovskite solar cells. *ACS Energy Lett.* **2019**, *4*, 1930−1937.

(2) Gao, W.; Chen, C.; Ran, C.; Zheng, H.; Dong, H.; Xia, Y.; Chen, Y.; Huang, W. A-Site Cation Engineering of Metal Halide Perovskites: Version 3.0 of Efficient Tin-Based Lead-Free Perovskite Solar Cells. *Adv. Funct. Mater.* **2020**, *30* (34), 2000794.

(3) Wu, T.; Liu, X.; Luo, X.; Lin, X.; Cui, D.; Wang, Y.; Segawa, H.; Zhang, Y.; Han, L. Lead-Free Tin Perovskite Solar Cells. *Joule* **2021**, *5* (4), 863−886.

(4) Kim, G.-H.; Kim, D. S. Development of Perovskite Solar Cells with > 25% Conversion Efficiency. *Joule* **2021**, *5* (5), 1033−1035.

(5) Jiang, X.; Li, H.; Zhou, Q.; Wei, Q.; Wei, M.; Jiang, L.; Wang, Z.; Peng, Z.; Wang, F.; Zang, Z.; Xu, K.; Hou, Y.; Teale, S.; Zhou, W.; Si, R.; Gao, X.; Sargent, E. H.; Ning, Z. One-Step Synthesis of SnI2·(DMSO)x Adducts for High-Performance Tin Perovskite Solar Cells. *J. Am. Chem. Soc.* **2021**, *143* (29), 10970−10976.

(6) Yu, B.-B.; Chen, Z.; Zhu, Y.; Wang, Y.; Han, B.; Chen, G.; Zhang, X.; Du, Z.; He, Z. Heterogeneous 2D/3D Tin-Halides Perovskite Solar Cells with Certified Conversion Efficiency Breaking 14%. *Adv. Mater.* **2021**, *33* (36), 2102055.

(7) Jokar, E.; Chaung, H.-S.; Kuan, C.-H.; Wu, H.-P.; Hou, C.-H.; Shyue, J.-J.; Diau, E. W.-G. Slow Passivation and Inverted Hysteresis for Hybrid Tin Perovskite Solar Cells Attaining 13.5% via Sequential Deposition. *J. Phys. Chem. Lett.* **2021**, *12*, 10106−10111.

(8) Liu, X.; Yan, K.; Tan, D.; Liang, X.; Zhang, H.; Huang, W. Solvent Engineering Improves Efficiency of Lead-Free Tin-Based Hybrid Perovskite Solar Cells beyond 9%. *ACS Energy Lett.* **2018**, *3* (11), 2701−2707.

(9) Shahbazi, S.; Li, M.-Y.; Fathi, A.; Diau, E. W.-G. Realizing a Cosolvent System for Stable Tin-Based Perovskite Solar Cells Using a Two-Step Deposition Approach. *ACS Energy Lett.* **2020**, *5* (8), 2508−2511.

(10) Kumar, M. H.; Dharani, S.; Leong, W. L.; Boix, P. P.; Prabhakar, R. R.; Baikie, T.; Shi, C.; Ding, H.; Ramesh, R.; Asta, M.; Graetzel, M.; Mhaisalkar, S. G.; Mathews, N. Lead-Free Halide Perovskite Solar Cells with High Photocurrents Realized through Vacancy Modulation. *Adv. Mater.* **2014**, *26* (41), 7122−7127.

(11) Jokar, E.; Chien, C.-H.; Fathi, A.; Rameez, M.; Chang, Y.-H.; Diau, E. W.-G. Slow Surface Passivation and Crystal Relaxation with Additives to Improve Device Performance and Durability for Tin-Based Perovskite Solar Cells. *Energy Environ. Sci.* **2018**, *11* (9), 2353−2362.

(12) Wang, C.; Gu, F.; Zhao, Z.; Rao, H.; Qiu, Y.; Cai, Z.; Zhan, G.; Li, X.; Sun, B.; Yu, X.; Zhao, B.; Liu, Z.; Bian, Z.; Huang, C. Self-Repairing Tin-Based Perovskite Solar Cells with a Breakthrough Efficiency Over 11%. *Adv. Mater.* **2020**, *32* (31), 1907623.

(13) Tai, Q.; Guo, X.; Tang, G.; You, P.; Ng, T. W.; Shen, D.; Cao, J.; Liu, C. K.; Wang, N.; Zhu, Y.; Lee, C. S.; Yan, F. Antioxidant Grain Passivation for Air-Stable Tin-Based Perovskite Solar Cells. *Angew. Chem., Int. Ed.* **2019**, *58* (3), 806−810.

(14) Zhao, Z.; Gu, F.; Li, Y.; Sun, W.; Ye, S.; Rao, H.; Liu, Z.; Bian, Z.; Huang, C. Mixed-Organic-Cation Tin Iodide for Lead-Free Perovskite Solar Cells with an Efficiency of 8.12%. *Adv. Sci.* **2017**, *4* (11), 1700204.

(15) Shao, S.; Liu, J.; Portale, G.; Fang, H. H.; Blake, G. R.; ten Brink, G. H.; Koster, L. J. A.; Loi, M. A. Highly Reproducible Sn-Based Hybrid Perovskite Solar Cells with 9% Efficiency. *Adv. Energy Mater.* **2018**, *8* (4), 1702019.

(16) Liao, Y.; Liu, H.; Zhou, W.; Yang, D.; Shang, Y.; Shi, Z.; Li, B.; Jiang, X.; Zhang, L.; Quan, L. N.; Quintero-Bermudez, R.; Sutherland, B. R.; Mi, Q.; Sargent, E. H.; Ning, Z. Highly Oriented Low-Dimensional Tin Halide Perovskites with Enhanced Stability and Photovoltaic Performance. *J. Am. Chem. Soc.* **2017**, *139* (19), 6693−6699.

(17) Jokar, E.; Chien, C. H.; Tsai, C. M.; Fathi, A.; Diau, E. W. G. Robust Tin-Based Perovskite Solar Cells with Hybrid Organic Cations to Attain Efficiency Approaching 10%. *Adv. Mater.* **2019**, *31* (2), 1804835.

(18) Jokar, E.; Hou, P.; Bhosale, S. S.; Chuang, H.; Narra, S.; Diau, E. W.-G. Mixing of Azetidinium in Formamidinium Tin Triiodide Perovskite Solar Cells for Enhanced Photovoltaic Performance and High Stability in Air. *ChemSusChem* **2021**, *14*, 4415−4421.

(19) Jokar, E.; Cheng, P.-Y.; Lin, C.-Y.; Narra, S.; Shahbazi, S.; Wei-Guang Diau, E. Enhanced Performance and Stability of 3D/2D Tin Perovskite Solar Cells Fabricated with a Sequential Solution Deposition. *ACS Energy Lett.* **2021**, *6* (2), 485−492.

(20) Liu, M.; Pasanen, H.; Ali-Löytty, H.; Hiltunen, A.; Lahtonen, K.; Qudsia, S.; Smått, J.-H.; Valden, M.; Tkachenko, N. V.; Vivo, P. B-Site Co-Alloying with Germanium Improves the Efficiency and Stability of All-Inorganic Tin-Based Perovskite Nanocrystal Solar Cells. *Angew. Chem., Int. Ed.* **2020**, *59* (49), 22117−22125.

(21) Tsai, C. M.; Mohanta, N.; Wang, C. Y.; Lin, Y. P.; Yang, Y. W.; Wang, C. L.; Hung, C. H.; Diau, E. W.-G. Formation of Stable Tin Perovskites Co-Crystallized with Three Halides for Carbon-Based Mesoscopic Lead-Free Perovskite Solar Cells. *Angew. Chem., Int. Ed.* **2017**, *56* (44), 13819−13823.

(22) Rameez, M.; Lin, E. Y.-R.; Raghunath, P.; Narra, S.; Song, D.; Lin, M.-C.; Hung, C.-H.; Diau, E. W.-G. Development of Hybrid Pseudohalide Tin Perovskites for Highly Stable Carbon-Electrode Solar Cells. *ACS Appl. Mater. Interfaces* **2020**, *12*, 21739−21747.

(23) Lee, S. J.; Shin, S. S.; Kim, Y. C.; Kim, D.; Ahn, T. K.; Noh, J. H.; Seo, J.; Seok, S., Il Fabrication of Efficient Formamidinium Tin Iodide Perovskite Solar Cells through SnF2−Pyrazine Complex. *J. Am. Chem. Soc.* **2016**, *138* (12), 3974−3977.

(24) Hao, F.; Stoumpos, C. C.; Guo, P.; Zhou, N.; Marks, T. J.; Chang, R. P. H.; Kanatzidis, M. G. Solvent-Mediated Crystallization of CH3NH3SnI3 Films for Heterojunction Depleted Perovskite Solar Cells. *J. Am. Chem. Soc.* **2015**, *137* (35), 11445−11452.

(25) Di Girolamo, D.; Pascual, J.; Aldamasy, M. H.; Iqbal, Z.; Li, G.; Radicchi, E.; Li, M.; Turren-Cruz, S.-H.; Nasti, G.; Dallmann, A.; De Angelis, F.; Abate, A. Solvents for Processing Stable Tin Halide Perovskites. *ACS Energy Lett.* **2021**, *6* (3), 959−968.

(26) Jiang, X.; Wang, F.; Wei, Q.; Li, H.; Shang, Y.; Zhou, W.; Wang, C.; Cheng, P.; Chen, Q.; Chen, L.; Ning, Z. Ultra-High Open-Circuit Voltage of Tin Perovskite Solar Cells via an Electron Transporting Layer Design. *Nat. Commun.* **2020**, *11* (1), 1245.

(27) Vegiraju, S.; Ke, W.; Priyanka, P.; Ni, J.-S.; Wu, Y.-C.; Spanopoulos, I.; Yau, S. L.; Marks, T. J.; Chen, M.-C.; Kanatzidis, M. G. Benzodithiophene Hole-Transporting Materials for Efficient Tin-Based Perovskite Solar Cells. *Adv. Funct. Mater.* **2019**, *29* (45), 1905393.

(28) Yun, J.-M.; Yeo, J.-S.; Kim, J.; Jeong, H.-G.; Kim, D.-Y.; Noh, Y.-J.; Kim, S.-S.; Ku, B.-C.; Na, S.-I. Solution-Processable Reduced Graphene Oxide as a Novel Alternative to PEDOT:PSS Hole

Transport Layers for Highly Efficient and Stable Polymer Solar Cells. *Adv. Mater.* **2011**, *23* (42), 4923−4928.
(29) Kung, P.-K.; Li, M.-H.; Lin, P.-Y.; Chiang, Y.-H.; Chan, C.-R.; Guo, T.-F.; Chen, P. A Review of Inorganic Hole Transport Materials for Perovskite Solar Cells. *Adv. Mater. Interfaces* **2018**, *5* (22), 1800882.
(30) Sapkota, S. B.; Fischer, M.; Zimmermann, B.; Würfel, U. Analysis of the Degradation Mechanism of ITO-Free Organic Solar Cells under UV Radiation. *Sol. Energy Mater. Sol. Cells* **2014**, *121*, 43−48.
(31) Ulman, A. Formation and Structure of Self-Assembled Monolayers. *Chem. Rev.* **1996**, *96* (4), 1533−1554.
(32) Hotchkiss, P. J.; Jones, S. C.; Paniagua, S. A.; Sharma, A.; Kippelen, B.; Armstrong, N. R.; Marder, S. R. The Modification of Indium Tin Oxide with Phosphonic Acids: Mechanism of Binding, Tuning of Surface Properties, and Potential for Use in Organic Electronic Applications. *Acc. Chem. Res.* **2012**, *45* (3), 337−346.
(33) Kim, S. Y.; Cho, S. J.; Byeon, S. E.; He, X.; Yoon, H. J. Self-Assembled Monolayers as Interface Engineering Nanomaterials in Perovskite Solar Cells. *Adv. Energy Mater.* **2020**, *10* (44), 2002606.
(34) Donley, C.; Dunphy, D.; Paine, D.; Carter, C.; Nebesny, K.; Lee, P.; Alloway, D.; Armstrong, N. R. Characterization of Indium−Tin Oxide Interfaces Using X-Ray Photoelectron Spectroscopy and Redox Processes of a Chemisorbed Probe Molecule: Effect of Surface Pretreatment Conditions. *Langmuir* **2002**, *18* (2), 450−457.
(35) Gonçalves, G.; Elangovan, E.; Barquinha, P.; Pereira, L.; Martins, R.; Fortunato, E. Influence of Post-Annealing Temperature on the Properties Exhibited by ITO, IZO and GZO Thin Films. *Thin Solid Films* **2007**, *515* (24), 8562−8566.
(36) Al-Ashouri, A.; Magomedov, A.; Roß, M.; Jošt, M.; Talaikis, M.; Chistiakova, G.; Bertram, T.; Márquez, J. A.; Köhnen, E.; Kasparavičius, E.; Levcenco, S.; Gil-Escrig, L.; Hages, C. J.; Schlatmann, R.; Rech, B.; Malinauskas, T.; Unold, T.; Kaufmann, C. A.; Korte, L.; Niaura, G.; Getautis, V.; Albrecht, S. Conformal Monolayer Contacts with Lossless Interfaces for Perovskite Single Junction and Monolithic Tandem Solar Cells. *Energy Environ. Sci.* **2019**, *12* (11), 3356−3369.
(37) Al-Ashouri, A.; Kohnen, E.; Li, B.; Magomedov, A.; Hempel, H.; Caprioglio, P.; Marquez, J. A.; Morales Vilches, A. B.; Kasparavicius, E.; Smith, J. A.; Phung, N.; Menzel, D.; Grischek, M.; Kegelmann, L.; Skroblin, D.; Gollwitzer, C.; Malinauskas, T.; Jost, M.; Matic, G.; Rech, B.; Schlatmann, R.; Topic, M.; Korte, L.; Abate, A.; Stannowski, B.; Neher, D.; Stolterfoht, M.; Unold, T.; Getautis, V.; Albrecht, S. Monolithic Perovskite/Silicon Tandem Solar Cell with > 29% Efficiency by Enhanced Hole Extraction. *Science* **2020**, *370* (6522), 1300−1309.
(38) Koch, N.; Elschner, A.; Rabe, J. P.; Johnson, R. L. Work Function Independent Hole-Injection Barriers Between Pentacene and Conducting Polymers. *Adv. Mater.* **2005**, *17* (3), 330−335.
(39) Karagkiozaki, V.; Karagiannidis, P. G.; Gioti, M.; Kavatzikidou, P.; Georgiou, D.; Georgaraki, E.; Logothetidis, S. Bioelectronics Meets Nanomedicine for Cardiovascular Implants: PEDOT-Based Nanocoatings for Tissue Regeneration. *Biochim. Biophys. Acta, Gen. Subj.* **2013**, *1830* (9), 4294−4304.
(40) Würfel, U.; Neher, D.; Spies, A.; Albrecht, S. Impact of Charge Transport on Current−Voltage Characteristics and Power-Conversion Efficiency of Organic Solar Cells. *Nat. Commun.* **2015**, *6* (1), 6951.
(41) Song, D.; Hsu, L. Y.; Tseng, C.-M.; Diau, E. W.-G. Solution-Processed ITO Nanoparticles as Hole-Selective Electrodes for Mesoscopic Lead-Free Perovskite Solar Cells. *Mater. Adv.* **2021**, *2* (2), 754−759.
(42) Karpovich, D. S.; Blanchard, G. J. Direct Measurement of the Adsorption Kinetics of Alkanethiolate Self-Assembled Monolayers on a Microcrystalline Gold Surface. *Langmuir* **1994**, *10* (9), 3315−3322.
(43) Paramonov, P. B.; Paniagua, S. A.; Hotchkiss, P. J.; Jones, S. C.; Armstrong, N. R.; Marder, S. R.; Brédas, J.-L. Theoretical Characterization of the Indium Tin Oxide Surface and of Its Binding Sites for Adsorption of Phosphonic Acid Monolayers. *Chem. Mater.* **2008**, *20* (16), 5131−5133.
(44) Gan, J.; Lu, X.; Wu, J.; Xie, S.; Zhai, T.; Yu, M.; Zhang, Z.; Mao, Y.; Wang, S. C. I.; Shen, Y.; Tong, Y. Oxygen Vacancies Promoting Photoelectrochemical Performance of In2O3 Nanocubes. *Sci. Rep.* **2013**, *3* (1), 1021.
(45) Lopez-Varo, P.; Jiménez-Tejada, J. A.; García-Rosell, M.; Ravishankar, S.; Garcia-Belmonte, G.; Bisquert, J.; Almora, O. Device Physics of Hybrid Perovskite Solar Cells: Theory and Experiment. *Adv. Energy Mater.* **2018**, *8* (14), 1702772.
(46) Shi, J.; Li, Y.; Li, Y.; Li, D.; Luo, Y.; Wu, H.; Meng, Q. From Ultrafast to Ultraslow: Charge-Carrier Dynamics of Perovskite Solar Cells. *Joule* **2018**, *2* (5), 879−901.
(47) De Bastiani, M.; Subbiah, A. S.; Aydin, E.; Isikgor, F. H.; Allen, T. G.; De Wolf, S. Recombination Junctions for Efficient Monolithic Perovskite-Based Tandem Solar Cells: Physical Principles, Properties, Processing and Prospects. *Mater. Horiz.* **2020**, *7* (11), 2791−2809.

https://doi.org/10.1021/acsenergylett.1c02124
ACS Energy Lett. 2021, 6, 4179−4186